Theoretical investigation of the lithium 2 p ← 2 s photoabsorption spectra perturbed by atomic hydrogen

N. Lamoudi, M. Bouledroua, K. Alioua, Abdul-Rahman Allouche, Monique Aubert-Frécon

Theoretical investigation of the lithium $2p \leftarrow 2s$ photoabsorption spectra perturbed by atomic hydrogen

N. Lamoudi,[1] M. Bouledroua,[2] K. Alioua,[2,3] A.-R. Allouche,[4] and M. Aubert-Frécon[4]

[1]*Physics Department, Badji Mokhtar University, B.P. 12 Annaba, Algeria*

[2]*Laboratoire de Physique des Rayonnements, Badji Mokhtar University, B.P. 12, Annaba 23000, Algeria*

[3]*Chérif Messadia University, B.P. 1553, Souk-Ahras 41000, Algeria*

[4]*Institut Lumière Matière, UMR5306 Université Lyon 1-CNRS, Université de Lyon, 69622 Villeurbanne Cedex, France*

(Received 19 February 2013; published 28 May 2013)

This work proposes a theoretical study of the Li($2p \leftarrow 2s$) photoabsorption spectra perturbed by ground hydrogen atoms. The temperature effect on the far-wing spectra is examined in the temperature range 4000–20 000 K. For this purpose, the ground and excited LiH potential curves and the transition dipole moments that connect them are constructed from *ab initio* data. The investigation shows that the profile spectra are dominated at all temperatures by the singlet $A \leftarrow X$ transitions and exhibit in the red wing a satellite structure near the wavelength 1000 nm. The spectra revealed also the appearance beyond 14 000 K of a second satellite structure in the blue wing close to the wavelength 510 nm originating from the triplet $c \leftarrow a$ transitions.

DOI: 10.1103/PhysRevA.87.052713 PACS number(s): 34.50.Gb, 34.90.+q, 31.50.Df, 32.70.Jz

I. INTRODUCTION

Over the last decades, lithium hydride dimer, LiH, and its various excited and ionized forms received extensive attention [1–4] and have continued to be the subject of numerous investigations during the past few years [5–9]. The cumbersome physical and chemical studies on this molecular system are primarily due to its particular interest in several fields, such as astrophysics and astrochemistry. Indeed, the lithium hydride molecule, which is widespread in the interstellar medium, played an important role in the early universe chemistry and contributed to the cooling of the primordial gas. Furthermore, the large dipole moment of the LiH system makes this hydride suitable for studying the early universe evolution and detecting the primary clouds [8–15].

To our knowledge, the pressure-broadened spectrum of lithium atoms evolving in a hydrogen bath has not been explored in the past, neither experimentally nor theoretically. We thus propose in this work to carry out *full* quantum-mechanical calculations of the far-wing absorption profile of the lithium ^{7}Li($2p \leftarrow 2s$) resonance line broadened by collisions with ground hydrogen ^{1}H($1s$) atoms at various temperatures. To fulfill this task, we first start by building up the interaction potentials, through which Li($2p \leftarrow 2s$) approaches H($1s$), and the needed transition dipole moments (TDMs). The quality of the constructed potentials and dipole moments will be assessed by comparing, with whatever available theoretical or experimental data, the radiative lifetimes of some excited Li($2p$) − H($1s$) rotational-vibrational levels and the temperature-dependent rate coefficients for radiative association of Li($2s/2p$) and H($1s$) to form the ground LiH molecule. We will then compute numerically the photoabsorption coefficients to study the satellite features in the *blue* and *red* wings of the LiH absorption profile and to examine their behavior with temperature.

Throughout this paper, all the physical data are expressed in atomic units, a.u., unless otherwise specified.

II. THEORY

We propose in the present work a quantum-mechanical investigation of the pressure-broadening phenomena which affect the far-wing photoabsorption spectra of lithium Li($2p \leftarrow 2s$) perturbed by ground hydrogen H($1s$) atoms. Such a spectral broadening occurs when the radiator Li absorbs a photon and interacts simultaneously with the disturbing atom H [16,17]. During this process, the formed LiH dimer goes under supposed conditions from its ground state dissociating into Li($2s$) + H($1s$) to its first excited states dissociating into Li($2p$) + H($1s$). The phenomenon is quantified in molecular spectroscopy by means of the absorption coefficient $k(\nu,T)$ at temperature T, with ν being the frequency of the absorbed photon.

In the following, we calculate the *reduced* photoabsorption coefficient $k_r(\nu,T)$ defined as the ratio

$$k_r(\nu,T) = \frac{k(\nu,T)}{[\mathrm{Li}]\,[\mathrm{H}]} \tag{1}$$

of the absorption coefficient and the lithium and hydrogen number densities, noted here [Li] and [H]. Generally, the photoabsorption coefficient of an allowed molecular transition is the sum of four absorption coefficients corresponding to four possible transitions, namely, *bound-bound* (b-b), *bound-free* (b-f), *free-bound* (f-b), and *free-free* (f-f), between two electronic states labeled by the vibrational and rotational quantum numbers, v and J, the projection Λ of the total electronic orbital angular momentum on the internuclear axis, and the energy ϵ for the case of free states. In this study, we utilize the reduced photoabsorption coefficients as formulated by Chung *et al.* [18]. Note that the values of the angular momentum quantum numbers used in the computations described below, J' and J'', respectively, for the *upper* and *lower* molecular states, are generally high. Hence, one may assume as valid the approximation $J' \simeq J'' = J$.

The *bound-bound* reduced absorption coefficient for transitions from the lower vibrational-rotational states

$\xi'' = (v'' J \Lambda'')$ to the upper vibrational-rotational states $\xi' = (v' J \Lambda')$ is [18]

$$k_r^{\text{b-b}}(\nu,T) = \frac{1}{h} C(\nu,T) \sum_{v'' J} \sum_{v'} g(\nu - \nu_{\text{tr}})(2J+1) \times M^2_{v'' J \Lambda'', v' J \Lambda'} \exp\left(-\frac{E_{v'' J \Lambda''}}{k_{\text{B}} T}\right), \quad (2)$$

where the factor $C(\nu,T)$ is

$$C(\nu,T) = \frac{8\pi^3 \nu}{3c} \varpi \left(\frac{2\pi\hbar^2}{\mu k_{\text{B}} T}\right)^{3/2}. \quad (3)$$

The symbols c and $h = 2\pi\hbar$ have their usual meaning, k_{B} is the Boltzmann constant, μ is the reduced mass of the radiator-perturber system LiH, and ϖ is the probability the lithium and hydrogen atoms form a molecule in the lower electronic state. The latter is given by

$$\varpi = \frac{2 - \delta_{0,\Lambda'+\Lambda''}}{2 - \delta_{0,\Lambda''}} \frac{2S_{\text{LiH}} + 1}{(2S_{\text{Li}} + 1)(2S_{\text{H}} + 1)}, \quad (4)$$

where δ is the well-known Kronecker symbol and S_{LiH}, S_{Li}, and S_{H} are the spin multiplicities for the LiH molecule and the Li and H atoms. The line-shape function $g(\nu - \nu_{\text{tr}})$ is replaced in this problem by the inverse of frequency bin size, and the *bound-bound* transition frequency ν_{tr} can be derived from the expression

$$h\nu_{\text{tr}} = E_{\xi'} - E_{\xi''} + h\nu_0, \quad (5)$$

where $E_{\xi'}$ and $E_{\xi''}$ are the rovibrational energies of the upper and lower electronic states, respectively, and $\nu_0 = 446.92$ THz is the Li($2s - 2p$) *atomic* transition frequency. The dipole matrix elements $M_{\xi'',\xi'}$ are defined as

$$M_{\xi'',\xi'} = \int_0^\infty \Phi_{\xi''}(R) D(R) \Phi_{\xi'}(R) dR, \quad (6)$$

with R being the internuclear separation and $D(R)$ the electronic transition dipole moment which correlates the initial and final states involved in the allowed transitions. Similarly, the remaining b-f, f-b, and f-f reduced absorption coefficients are expressed by the following set of formulas [18]:

$$k_r^{\text{b-f}}(\nu,T) = C(\nu,T) \sum_{v'' J} (2J+1) \times M^2_{v'' J \Lambda'', \epsilon' J \Lambda'} \exp\left(-\frac{E_{v'' J \Lambda''}}{k_{\text{B}} T}\right), \quad (7)$$

$$k_r^{\text{f-b}}(\nu,T) = C(\nu,T) \sum_{v' J} (2J+1) M^2_{\epsilon'' J \Lambda'', v' J \Lambda'} \exp\left(-\frac{\epsilon''}{k_{\text{B}} T}\right), \quad (8)$$

$$k_r^{\text{f-f}}(\nu,T) = C(\nu,T) \sum_J \int d\epsilon' (2J+1) \times M^2_{\epsilon'' J \Lambda'', \epsilon' J \Lambda'} \exp\left(-\frac{\epsilon''}{k_{\text{B}} T}\right). \quad (9)$$

The *energy*- and *space*-normalized radial wave functions in Eq. (6), $\Phi_\xi = \Phi_{\epsilon J \Lambda}(R)$ and $\Phi_\xi = \Phi_{v J \Lambda}(R)$, respectively, are the solution of the radial wave equation

$$\frac{d^2\Phi_\xi(R)}{dR^2} + \frac{2\mu}{\hbar^2}\left[\mathcal{E} - V_\Lambda(R) - \frac{\hbar^2}{2\mu}\frac{J(J+1) - \Lambda^2}{R^2}\right] \times \Phi_\xi(R) = 0, \quad (10)$$

where $V(R) = V_\Lambda(R)$ is the interatomic potential energy with $\Lambda = 0$ for Σ states and $\Lambda = 1$ for Π states. The energy $\mathcal{E} = \epsilon$ is *positive* for the continuous free states and $\mathcal{E} = E$ is *negative* for the discrete bound states.

According to the above relationships (2) and (7)–(9), the absorption coefficients can only be computed once the interatomic potentials $V(R)$ and the transition dipole moments $D(R)$ are known in the entire range of the internuclear separation R.

III. POTENTIAL AND TDM CONSTRUCTIONS

At thermal equilibrium, the ground Li($2s$) and H($1s$) atoms interact mutually along the singlet $X\ ^1\Sigma^+$ or the triplet $a\ ^3\Sigma^+$ potential-energy curve, whereas the excited Li($2p$) interacts with the ground H($1s$) along one of the four possible excited molecular curves, namely, $A\ ^1\Sigma^+$, $B\ ^1\Pi$, $b\ ^3\Pi$, and $c\ ^3\Sigma^+$. In the present photoabsorption investigation, knowledge of the LiH potentials in connection with the above six states is needed in the whole range of the interatomic distances. More precisely, the potentials are described in the short- and long-range regions using parametrized analytical forms, while in the intermediate distances they are determined from accurate and reliable *ab initio* calculations performed for several values of R.

In the intermediate range of internuclear distances, the LiH quasimolecule is treated as a two-active electron system, using a nonempirical pseudopotential, of the Durand and Barthelat type [19], to describe the Li atom. Core-polarization effects are included *via* a core-polarization potential (CPP) for the Li atom in the form first proposed by Müller and Meyer [20] and later revisited by Foucrault *et al.* [21]. For lithium, we used the Gaussian basis set and the CPP previously used in [22]. To describe the hydrogen atom, we used a basis set obtained from a cc-pv6z one slightly modified. The molecular orbitals of LiH are obtained from a self-consistent field calculation, and the electronic correlation between the two active electrons is taken into account through full configuration interaction (CI) calculations. All calculations were performed using the CIPSI code [23,24]. The computed energy points are smoothly connected in the short-range region to the Born-Mayer form $V_{\text{SR}}(R) = \alpha \exp(-\beta R)$ [25], with α and β being two parameters to be determined, and in the long-range region to the usual relationship $V_{\text{LR}}(R) = -C_6/R^6 - C_8/R^8 - C_{10}/R^{10}$, with C_n being the dispersion coefficients. In these constructions, we adopted the dispersion coefficients generated by Mitroy and collaborators [26,27] and Zhu *et al.* [28]. Their values are shown in Table I with the computed constants α and β.

To construct the $X\ ^1\Sigma^+$ molecular state, we used the *ab initio* points we have produced in the range $1.5 \leqslant R \leqslant 17a_0$. The upper singlet $A\ ^1\Sigma^+$ and $B\ ^1\Pi$ states are also constructed from the *ab initio* points computed over the same interval. The triplet energy curves rely on the *ab initio* data points in the intervals of R going from $1.5a_0$ to $17a_0$, for the $a\ ^3\Sigma^+$ and $b\ ^3\Pi$ states, and from $1.5a_0$ to $22a_0$, for the

TABLE I. Short- and long-range constant parameters (in a.u.) used in the construction of the ground and excited LiH potentials.

Dissociation limit	Molecular state	Short range α	Short range β	Long range C_6	Long range $10^{-3} \times C_8$	Long range $10^{-5} \times C_{10}$
Li(2s) + H(1s)	$X\ ^1\Sigma^+$	35.028	3.752	66.544[a]	3.2821[a]	2.2318[a]
	$a\ ^3\Sigma^+$	2.981	1.677	66.544[a]	3.2821[a]	2.2318[a]
Li(2p) + H(1s)	$A\ ^1\Sigma^+$	4.921	2.184	160.1 [b]	24.04 [b]	28.12[b]
	$B\ ^1\Pi$	3.574	1.828	85.418[c]	1.143 [b]	
	$b\ ^3\Pi$	4.133	1.995	85.418[c]	1.143[b]	
	$c\ ^3\Sigma^+$	2.970	1.600	160.1[b]	24.04[b]	

[a]Reference [26].
[b]Reference [27].
[c]Reference [28].

$c\ ^3\Sigma^+$ state. In all cases, we kept in mind the so-called Le Roy criterion [29], which suggests to apply the $\sum_n C_n/R^n$ expansion beyond the Le Roy radii $R \gtrsim 12a_0$ and $R \gtrsim 14a_0$ for the $^1\Sigma^+$ and $^3\Sigma^+$ interactions [30]. The obtained hybrid singlet and triplet potential-energy curves are plotted in part (a) of Fig. 1. Some of the theoretical and Rydberg-Klein-Rees (RKR) data points produced by Geum *et al.* [31,32] and Coxon and Dickinson [33,34] are also presented for comparison. The well-known spectroscopic constants (the potential well depth D_e, the equilibrium distance R_e, and the minimum-to-minimum electronic excitation energy T_e) deduced from the constructed potentials are tabulated in Table II. They are also compared with experimental and theoretical data when available. The present description of the $^1\Sigma^+$ states is seen to be accurate when compared to the measured and computed R_e and D_e values [34–36], while the $^{1,3}\Pi$ states seem to be less accurate, especially for the D_e values for which the relative differences may reach 10%. Furthermore, present calculations predict the $^3\Sigma^+$ states to be slightly bound. In fact, most of the previous theoretical investigations predicted these states to be mainly repulsive, though the $a\ ^3\Sigma^+$ state is revealed to be shallower from two different theoretical investigations [37,38].

To see how accurate the constructed potentials are, it is interesting to examine the LiH vibrational levels of each electronic state. We could detect 24, 27, and 3 rotationless vibrational levels for the $X\ ^1\Sigma^+$, $A\ ^1\Sigma^+$, and $B\ ^1\Pi$ states, respectively. For these three states, we compare in Table III the vibrational energy level differences $\Delta G_v = G_{v+1} - G_v$. Our values are, in general, quite well consistent with the published

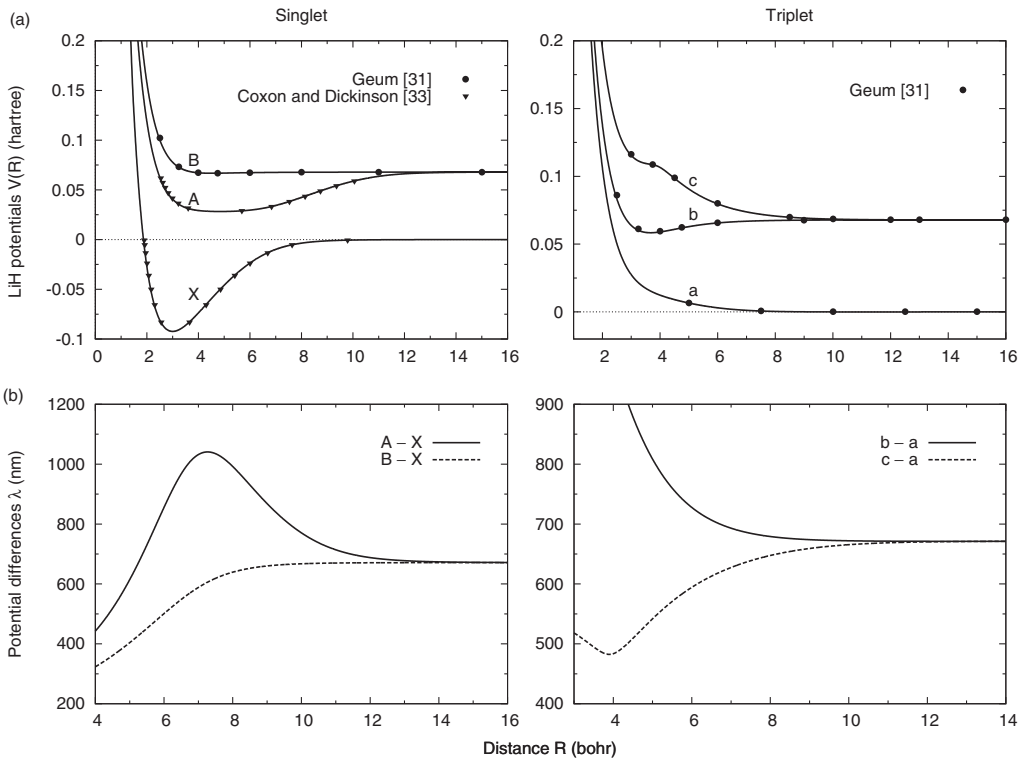

FIG. 1. Potential-energy curves (Part a) and potential differences (Part b) relative to the Li(2s) + H(1s) and Li(2p) + H(1s) dimers. Present potential curves of the $X\ ^1\Sigma^+$ and $A\ ^1\Sigma^+$ states are compared with the RKR values from [33]. The singlet $B\ ^1\Pi$ and all the triplet curves are compared with *ab initio* points from [31]. The potential differences are transformed into wavelengths, given in nanometers.

TABLE II. Spectroscopic constants of the ground and excited LiH potentials compared with experimental and theoretical values.

LiH states	D_e (cm^{-1})	R_e (a_0)	T_e (cm^{-1})	Refs.
$X\ ^1\Sigma^+$	20269.2	3.000		This work
	20286.0	3.015		[33][a]
	20287.7 ± 0.3	3.015		[35][a]
	20349.4	3.003		[36][b]
$a\ ^3\Sigma^+$	6.90	11.053	35168.97	This work
	4.2	11.527		[37][b]
	4.84	11.369		[38][b]
$A\ ^1\Sigma^+$	8704.2	4.840	26471.73	This work
	8680.7	4.908		[33][a]
	8681.6 ± 0.3	4.906	26509.77	[35][a]
	8686.6	4.862		[36][b]
$B\ ^1\Pi$	255.05	4.520	34920.83	This work
	288.9 ± 0.3	4.504	34902.84	[35][a]
	258.10	4.524	34821	[39][b]
$b\ ^3\Pi$	2084.04	3.673	33091.82	This work
	1822.81	3.693		[4][b]
	2083	3.677	32990	[39][b]
$c\ ^3\Sigma^+$	2.77527	15.147	35173.11	This work

[a]Experimental.
[b]Theoretical.

TABLE IV. Rotationless vibrational energy levels, in cm^{-1}, of the triplet LiH molecular states.

v	$a\ ^3\Sigma^+$	$c\ ^3\Sigma^+$	$b\ ^3\Pi$
0	−0.3002	−0.0106	−1179.5005
1			−1228.5501
2			−775.4053
3			−424.8452
4			−180.9808
5			−44.9808
6			−1.4071

experimental and computed data. Concerning the triplet states, the calculations yield seven bound levels for the $b\ ^3\Pi$ state and just one level for both $a\ ^3\Sigma^+$ and $c\ ^3\Sigma^+$ states. The results are listed in Table IV.

Moreover, we present in part (b) of Fig. 1 the four possible potential differences $V_{A-X}(R)$, $V_{B-X}(R)$, $V_{b-a}(R)$, and $V_{c-a}(R)$. According to the semiclassical theory [17], a satellite occurs when the potential-difference curve exhibits an extremum. The energy position of such an extremum, transformed in wavelengths, leads to the position of the satellite. Consequently, as one may note from Fig. 1(b), two satellites should arise, one in the red wing from the $A \leftarrow X$

TABLE III. Comparison of calculated and observed rotationless vibrational level spacing $\Delta G_v = G_{v+1} - G_v$, in cm^{-1}, among the singlet LiH molecular states.

	$X\ ^1\Sigma^+$			$A\ ^1\Sigma^+$			$B\ ^1\Pi$		
v	This work	[36][a]	[40][b]	This work	[36][a]	[30][b]	This work	[39][a]	[41][b]
0	1354.32	1355.81	1359.71	280.04	278.43	281.5	115.8086	117.07	130.76
1	1309.75	1311.43	1314.89	312.80	310.93	309.3	35.6473	34.18	44.97
2	1266.60	1267.93	1270.89	335.85	333.96	335.1			
3	1224.16	1225.25	1227.77	353.05	351.32	352.1			
4	1182.23	1183.28	1185.44	366.12	364.47	365.1			
5	1140.81	1141.93	1143.77	375.97	374.40	375.2			
6	1099.89	1101.05	1102.60	383.15	381.70	382.3			
7	1059.35	1060.46	1061.78	388.06	386.58	387.2			
8	1019.08	1020.00	1021.17	390.97	389.59	390.2			
9	978.60	979.43	980.52	392.12	390.79	391.7			
10	937.90	938.43	939.62	392.15	390.37	391.1			
11	896.54	896.77	898.09	389.78	388.55	389.9			
12	854.10	854.04	855.48	386.52	385.33	386.0			
13	810.02	809.68	811.19	381.97	380.82	381.8			
14	763.55	763.20	764.44	376.12	375.02	374.8			
15	713.72	713.69	714.22	368.93	367.88	367.7			
16	659.24	660.02	659.27	360.30	359.31	361.1			
17	598.43	600.82	597.89	350.03	349.11	352.3			
18	529.15	533.93	527.91	337.80	337.00	343.5			
19	448.80	456.87	446.61	323.13	322.47	327.1			
20	354.53	366.46	350.99	305.22	304.78	305.9			
21	243.97	259.59	237.71	282.89	282.75	284.0			
22	117.49			254.25	254.54	256.9			
23				216.28	217.49	219.5			
24				164.33	166.72	160.6			
25				92.37		74.9			

[a]Theoretical.
[b]Experimental.

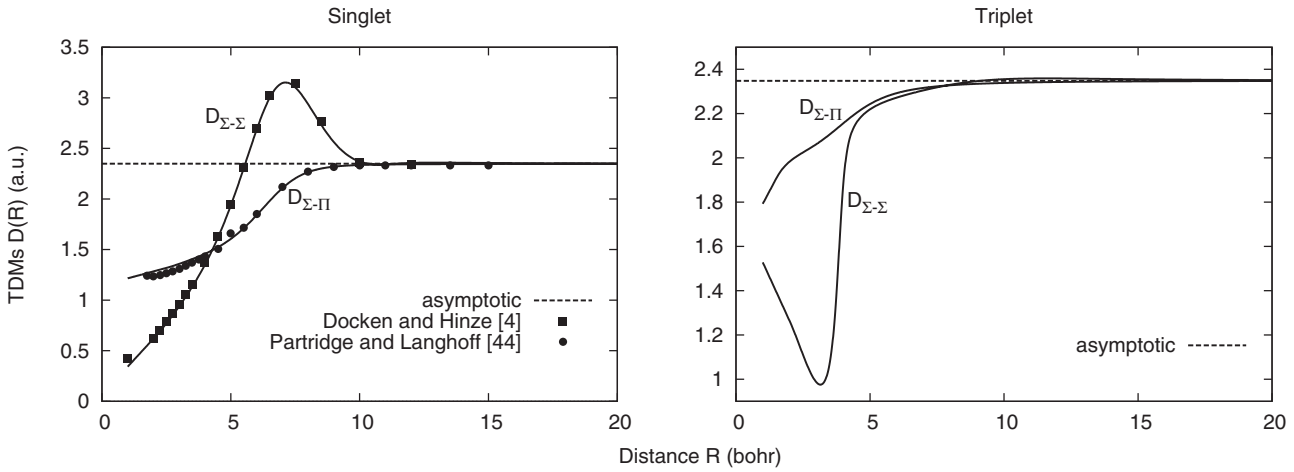

FIG. 2. Constructed singlet and triplet transition dipole moments $D(R)$. The singlet $\Sigma-\Sigma$ and $\Sigma-\Pi$ moments are compared with theoretical data from Docken and Hinze [4] and Partridge and Langhoff [44], respectively.

transitions near the wavelength $\lambda \sim 1040$ nm and another in the blue wing from the $b \leftarrow a$ transitions near the wavelength $\lambda \sim 482$ nm.

On the other hand, the transition dipole moments are constructed with a similar numerical procedure to that reported previously for the potential curves. We have calculated the *ab initio* TDM values in the intermediate region using the wave functions obtained with the method described above. For short and long distances, the TDMs vary according to the analytical forms

$$D(R) \sim \begin{cases} a + bR \\ D_\infty + AR^{-3}, \end{cases} \tag{11}$$

respectively. Here, a, b, and A are constant parameters and D_∞ is the asymptotic value of $D(R)$. In order to obtain the values of D_∞ and A, we have fitted our computed long-range TDM data points to a form similar to Eq. (11). We have found $D_\infty = 2.348$, which is very close to the experimental value 2.350 of Wiese *et al.* [42] and to 2.343 used by Zemke and Stwalley [43]. We have also found $A = +24.956\,2$ and $A = -7.108\,9$ for the $\Sigma-\Sigma$ and $\Sigma-\Pi$ transitions, respectively. Figure 2 shows our constructed TDMs compared with published singlet $X \leftarrow A$ and $X \leftarrow B$ data from [4,44].

The potential-energy and TDM data points generated by our *ab initio* calculations can be provided on request.

IV. FURTHER POTENTIAL AND TDM ASSESSMENTS

Before any further use, it is important at this stage to properly assay the potential-energy curves and transition dipole moments we have generated above. To this end, we have chosen to look at the radiative lifetimes of the individual rotational-vibrational levels and the T-dependent rate coefficients for radiative association of Li($2s/2p$) and H($1s$) to form the LiH($X\ ^1\Sigma^+$) molecule.

A. Radiative lifetime

Assuming once again the approximation on the angular momenta, $J' \approx J'' = J$, the radiative lifetime $\tau = 1/\mathcal{A}(v'J\Lambda')$ is related to the total spontaneous emission rate

$$\mathcal{A}(v'J\Lambda') = \frac{64\pi^4}{3hc^3}\frac{2-\delta_{0,\Lambda'+\Lambda''}}{2-\delta_{0,\Lambda'}}\left[\int_0^\infty \nu^3_{v'J\Lambda',\epsilon''J\Lambda''} M^2_{v'J\Lambda',\epsilon''J\Lambda''} \times d\epsilon'' + \sum_{v''} \nu^3_{v'J\Lambda',v''J\Lambda''} M^2_{v'J\Lambda',v''J\Lambda''}\right], \tag{12}$$

corresponding to transitions from the upper bound level $\xi' = (v'J\Lambda')$ to all the lower continuum $\xi'' = (\epsilon''J\Lambda'')$ and bound $\xi'' = (v''J\Lambda'')$ states. In this equation, the first and second

TABLE V. Radiative lifetimes, in nanoseconds, of the LiH $A\,^1\Sigma^+$ and $B\,^1\Pi$ states compared with some computed and measured values from [43–47].

$A\ ^1\Sigma^+$ ($\Lambda' = 0$)					$B\ ^1\Pi$ ($\Lambda' = 1$)					
v'	J'	This work	[45][a]	[46][a]	v'	J'	This work	[47][a]	[43][b]	[44][b]
2	3	32.56	29.4 ± 1.3		0	0	10.80	11.4 ± 0.6	11.3	11.3
5	3	36.81	30.5 ± 1.3		1	0	18.31	17.0 ± 0.8	17.0	17.0
5	5	36.89		32.6 ± 4.2	2	0	25.86	23.4 ± 4.0	24.0	23.5
5	10	37.26		32.6 ± 3.0						
5	15	37.78		29.0 ± 3.2						
7	3	38.57	34.9 ± 1.9							
7	12	38.94	36.9 ± 1.9							
8	15	38.92		32.2 ± 5.9						

[a]Experimental.
[b]Theoretical.

TABLE VI. LiH rate coefficients $\alpha(T)$ for radiative association at various temperatures. All the data are compared with results from Gianturco and Gori Giorgi [53,54].

Temperature	$X\ ^1\Sigma^+ \leftarrow X\ ^1\Sigma^+$		$X\ ^1\Sigma^+ \leftarrow A\ ^1\Sigma^+$		$X\ ^1\Sigma^+ \leftarrow B\ ^1\Pi$	
T (K)	This work[a]	[54][a]	This work[b]	[53][b]	This work[c]	[53][c]
100	2.997	2.34	3.865	4.47	0.775	0.382
500	3.226	2.28	4.763	5.72	0.430	0.216
1000	2.686	1.66	4.954	5.75	0.339	0.174
1500	2.207	1.22	4.816	5.39	0.297	0.154
3000	1.321	0.61	4.097	4.30	0.239	0.130
5000	0.810	0.33	3.275	3.30	0.202	0.110
6000	0.675		2.950	2.90	0.189	0.099
7000	0.580		2.671	2.60	0.177	0.092
7500	0.543		2.546		0.171	
8000	0.511		2.430		0.166	

[a]In units 10^{-20} cm^3 s^{-1}.
[b]In units 10^{-16} cm^3 s^{-1}.
[c]In units 10^{-14} cm^3 s^{-1}.

terms represent the probabilities of the spontaneous *bound-free* and *bound-bound* emissions, respectively.

We compare in Table V the calculated $A\ ^1\Sigma^+$ and $B\ ^1\Pi$ lifetime values of some rovibrational levels $(v'J')$ with measurements and computations from [43–47]. It appears the presented results are in fair accordance with the experimental data, mainly for the higher levels. We have further attempted to estimate the *atomic* lifetime of the lithium $2s-2p$ transition by averaging all the possible transitional cases. This could be accomplished by considering the *highest* rotationless vibrational states close to the dissociation limit. In such a case, the atomic lifetime τ_a is the weighted sum

$$\frac{1}{\tau_a} = \frac{1}{4}\left[\frac{1}{3}\mathcal{A}(v'_{\max}00) + \frac{2}{3}\mathcal{A}(v'_{\max}01)\right] + \frac{3}{4}\left[\frac{1}{3}\mathcal{A}(v'_{\max}00) + \frac{2}{3}\mathcal{A}(v'_{\max}01)\right]. \quad (13)$$

The theoretical calculations we have carried out yielded the value 27.36 ns, which does not differ more than 1.4% from the measured values 27.22 ± 0.20 ns of Carlsson and Sturesson [48], 27.102 ± 0.009 ns of McAlexander *et al.* [49], and 27.11 ± 0.06 ns of Volz and Schmoranzer [50]. Most recently, improved atomic radiative lifetimes have been determined experimentally by Le Roy *et al.* [51], who found 27.1018 ± 0.0014 ns for ^{7}Li$(2p)$ and 27.1024 ± 0.0014 ns for ^{6}Li$(2p)$. All these data agree very closely with the NIST recommended value 27.11 ns [52].

B. Radiative association

The radiative association of lithium and hydrogen atoms to form the LiH molecule occurs *via* one of the following mechanisms [15]:

$$\mathrm{Li}(2s) + \mathrm{H}(1s) \longrightarrow \mathrm{LiH}(X\ ^1\Sigma^+) \longrightarrow \mathrm{LiH}(X\ ^1\Sigma^+) + h\nu \quad (\mathrm{I})$$

and/or

$$\mathrm{Li}(2p) + \mathrm{H}(1s) \longrightarrow \left\{\begin{matrix}\mathrm{LiH}(A\ ^1\Sigma^+)\\ \mathrm{LiH}(B\ ^1\Pi)\end{matrix}\right\} \longrightarrow \mathrm{LiH}(X\ ^1\Sigma^+) + h\nu. \quad (\mathrm{II})$$

Both processes induce spontaneous emission of photons and imply *free-bound* transitions between states associated to the

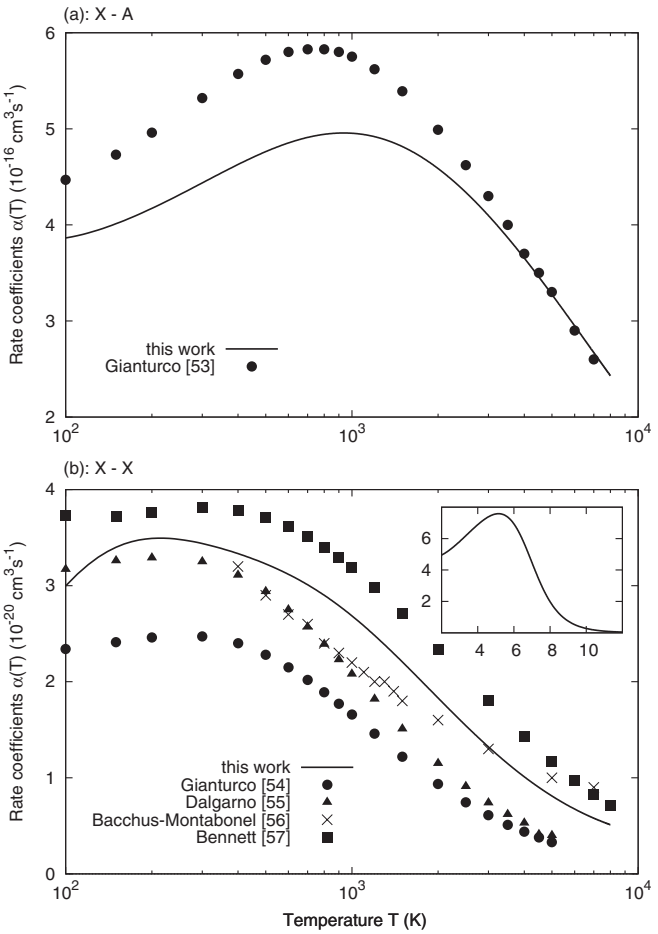

FIG. 3. Radiative association rate coefficients $\alpha(T)$ as a function of temperature for the $X \leftarrow A$ (part a) and the $X \leftarrow X$ (part b) transitions. The solid lines represent our results compared with values from published works [53–57]. The inset shows the LiH$(X\ ^1\Sigma^+)$ dipole moment versus the internuclear separation, both in a.u., from Partridge and Langhoff [44].

same potential-energy curve, like in scheme (I), or to two *distinct* potential curves, like in scheme (II). Gianturco and Gori Giorgi [53] found that the process (II) is, in this case, much more efficient than process (I).

A full quantum-mechanical theory yields the rate coefficients $\alpha(T)$ at temperature T as

$$\alpha(T) = \left(\frac{8}{\mu\pi}\right)^{1/2} \left(\frac{1}{k_B T}\right)^{3/2} \int_0^\infty \epsilon' Q(\epsilon') \exp\left(-\frac{\epsilon'}{k_B T}\right) d\epsilon'. \tag{14}$$

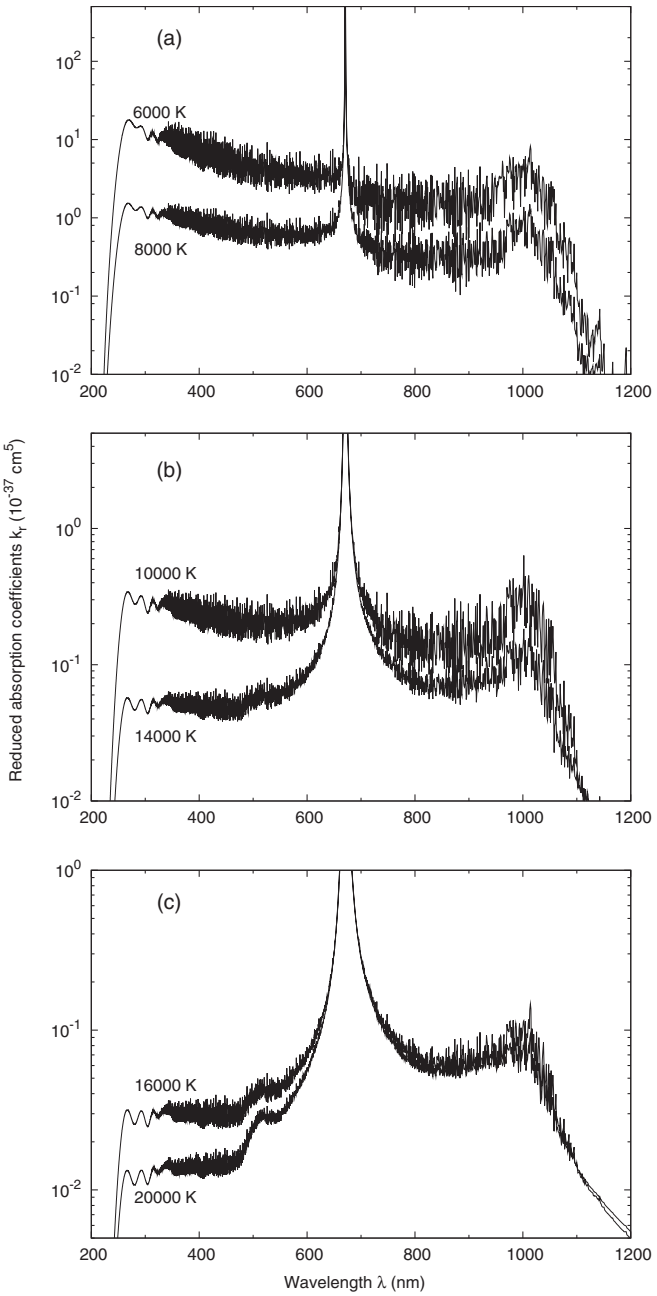

FIG. 4. LiH reduced photoabsorption coefficients for six temperatures ranging between 6000 and 20 000 K.

These coefficients are deduced by averaging the radiative association cross sections [53,54]

$$Q(\epsilon') = \frac{64\pi^5}{3c^3k^2} p \sum_{J'=0}^{J_{\max}} \sum_{v''=0}^{v_{\max}} \nu^3 \left[J' M^2_{v''J'\Lambda'',\epsilon'J'-1\Lambda'} + (J'+1) M^2_{v''J'\Lambda'',\epsilon'J'+1\Lambda'} \right] \tag{15}$$

over a Maxwellian velocity distribution. In this expression, $k = (2\mu\epsilon')^{\frac{1}{2}}/\hbar$ denotes the wave number of the colliding atoms and p is the statistical weight of the involved molecular transitions, which gets the values $p = 1/4$ for $X \leftarrow X$, $p = 1/12$ for $X \leftarrow A$, and $p = 1/6$ for $X \leftarrow B$.

Table VI gathers results of the LiH radiative association rate coefficients $\alpha(T)$ we gleaned from computations we have performed with the potentials and TDMs constructed in this work. The rates are given at some temperatures ranging from 100 to 8000 K relative to both schemes (I) and (II). They are also compared in the same table with values from [53,54]. One may notice that the rate coefficients in connection with the $X \leftarrow A$ transitions do not differ significantly, especially for $T \gtrsim 2000$ K, which can also be confirmed in Fig. 3(a). This is not the case with the other two recombination processes, $X \leftarrow X$ and $X \leftarrow B$, where the values deviate from the published data by a factor up to 3.

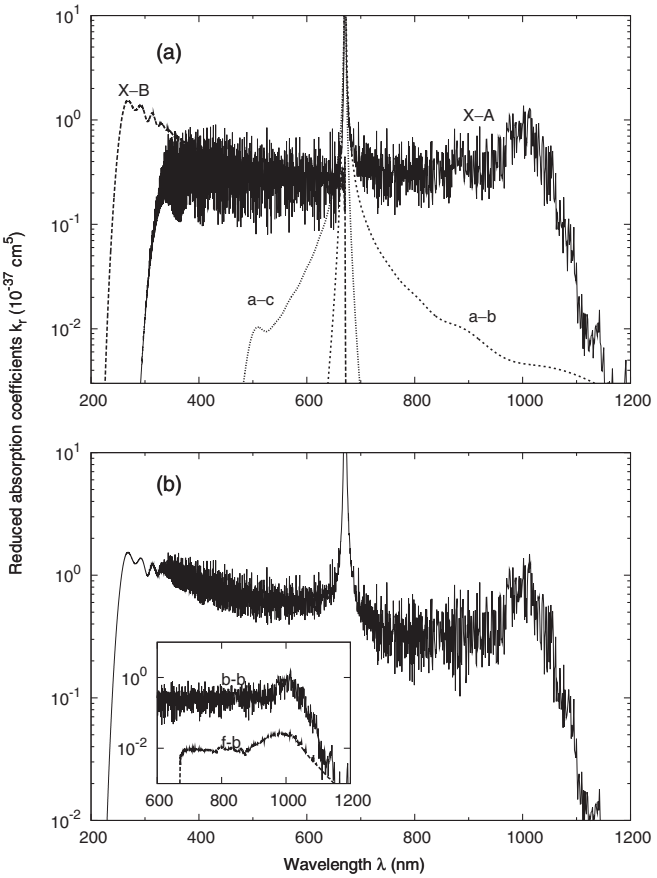

FIG. 5. LiH reduced photoabsorption coefficient at 8000 K. Part (a) displays the contribution of the $A \leftarrow X$, $B \leftarrow X$, $b \leftarrow a$, and $c \leftarrow a$ transitions and part (b) represents the sum of all the contributions. The inset shows the *bound-bound* and *free-bound* $A \leftarrow X$ transitions that contribute in the 1000-nm red satellite.

Nevertheless, as Fig. 3(b) illustrates, our higher temperature $X \leftarrow X$ results show good concordance with those already published in literature [54–57]. It is worth mentioning that we employed for the calculation of the $X\ ^1\Sigma^+ \leftarrow X\ ^1\Sigma^+$ rate coefficients the LiH R-dependent dipole moment, plotted in the inset of Fig. 3(b), determined theoretically by Partridge and Langhoff [44].

V. COMPUTATIONAL RESULTS AND DISCUSSION

The total LiH reduced absorption coefficient is the sum of the components corresponding to the *four* allowed transitions, namely, $A \leftarrow X$, $B \leftarrow X$, $c \leftarrow a$, and $b \leftarrow a$. Since both $X\ ^1\Sigma^+$ and $A\ ^1\Sigma^+$ states are characterized by relatively deep potentials, the $A \leftarrow X$ transition is then expected to contribute with all the possible b-b, b-f, f-b, and f-f transitions. Besides, the $B\ ^1\Pi$ potential well is very shallow. We can therefore neglect its three bound levels and consider only the f-f and b-f contributions in the $B \leftarrow X$ transition. Concerning now the LiH triplet states, the $a\ ^3\Sigma^+$ and $c\ ^3\Sigma^+$ potential-energy curves are mostly repulsive, whereas the $b\ ^3\Pi$ state has a deeper potential well. Accordingly, the main contributions to the total absorption coefficient come from the *free-free* $c \leftarrow a$ and $b \leftarrow a$ and *free-bound* $b \leftarrow a$ transitions.

Using Eqs. (2) and (7)–(9), we performed calculations for wavelengths and temperatures ranging from 200 to 1200 nm and from 4000 to 20 000 K, respectively, with a bin size $\Delta\nu = 10\ \mathrm{cm}^{-1}$. We believe at such temperatures the LiH interactions are perturbed by the presence of highly excited and ionized lithium or hydrogen atoms. Indeed, as pointed out by Krupenie *et al.* [2], the LiH molecule constitutes at 1500 K less than 5% of the Li + H mixture, and ionization reaches 5% at 6000 K. To obtain the bound and free wave functions required in the computation of the matrix elements (6), we solved numerically the radial wave equation (10) by adopting the Numerov algorithm. In particular, the Gauss-Laguerre quadrature, with 100 weighted points, has been used to compute the *free-free* integral appearing in Eq. (9). In order to simulate the photoabsorption spectra, we used in the calculations the maximum values of the rotational quantum number $J_{\max} = 250$ for the *free-free* transitions and $25 \leqslant J_{\max} \leqslant 98$ for the remaining transitions.

The results of the quantum-mechanical LiH absorption spectra, achieved for six distinct temperatures, are shown in Fig. 4. The total spectra display the *blue* and *red* branches in either sides of the Li $(2p \leftarrow 2s)$ atomic resonance line $\lambda_0 = 670.8$ nm. The profiles exhibit in the blue wing a satellite structure in the neighborhood of the wavelength $\lambda \sim 510$ nm, whereas the red wing shows a second satellite around the wavelength $\lambda \sim 1000$ nm. The former satellite starts its growth only beyond $T \gtrsim 14\,000$ K, but the latter appears for almost all temperatures of interest. The two wavelength values seem to be consistent with those already deduced from the potential differences discussed above, which predicted semiclassically the wavelengths 1040 and 482 nm.

Figure 5(a) displays the four partial contributions at $T = 8000$ K to the total spectrum plotted in Fig. 5(b). One may note, in particular, the dominance of the $A \leftarrow X$ transition at this temperature on the total spectral profile in both wings. This transition is responsible for the appearance of the 1000-nm satellite in the red wing, which is generated by the *bound-bound* and *free-bound* transitions, as demonstrated in Fig. 5(b) in the inset. The undulations are mainly due to

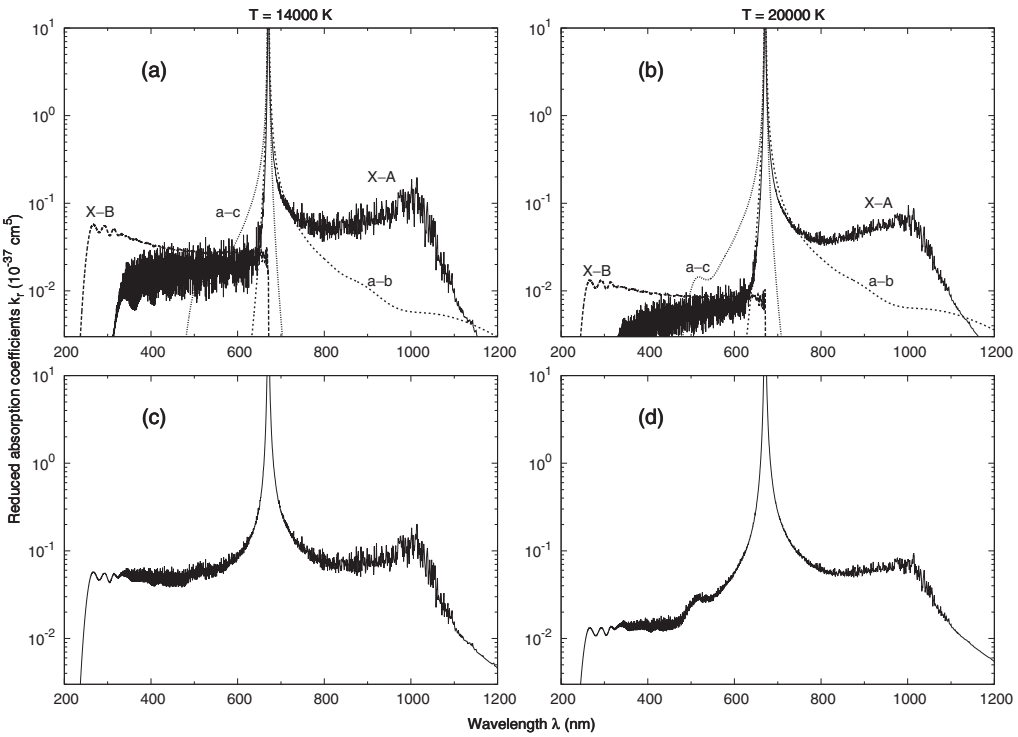

FIG. 6. LiH reduced photoabsorption coefficients at temperatures 14 000 and 20 000 K. Parts (a) and (b) display the contribution of the different transitions to the spectra, while parts (c) and (d) display the sum of all the contributions.

the abundance of bound levels involved in the *bound-bound* $A \leftarrow X$ transition, since both $X\ ^1\Sigma^+$ and $A\ ^1\Sigma^+$ LiH states possess very deep potential wells. Figure 5(a) also displays the contribution of the $B \leftarrow X$ transition, characterized by smooth undulations, which dominates the blue wing only. On the other hand, the $c \leftarrow a$ transition has practically no effects on the overall shape of the total spectrum at this temperature. Its contribution is limited to the creation of the satellite located in the blue wing around $\lambda \sim 510$ nm. As Fig. 5(a) shows, the intensity of this satellite is almost a hundred times weaker than those originating from the $A \leftarrow X$ and $B \leftarrow X$ transitions, but its importance should arise at higher temperatures, as it is going to be seen below. The $b \leftarrow a$ transition, solely present in the red wing, has almost no influence over the general shape of the spectral profile. Moreover, we present in Fig. 6 the contributions of the different transitions at higher temperatures, namely, 14 000 and 20 000 K. At such temperatures, the intensities of both $A \leftarrow X$ and $B \leftarrow X$ absorption coefficients decrease substantially and become of the same order of magnitude as the intensity corresponding to the $c \leftarrow a$ transition. The 510-nm satellite arising from this band begins to appear in the total spectra plotted in Fig. 6(b) at about 14 000 K and becomes, as stated above, noticeable beyond this temperature [Figs. 4(c) and 6(d)].

It emerges from the above discussion that there is an important effect of temperature on the general shape and behavior of the photoabsorption spectra. Indeed, one may notice that the influence of temperature on the blue wing is more remarkable than on the red wing. The rate of intensity change in both wings is not the same as the temperature increases, and the blue wing is more affected. Figure 7 exhibits the 1000- and 510-nm satellite peaks and displays their modification in magnitude with temperature when T goes from 4000 to 14 000 K. According to Fig. 7(a), the amplitude of the undulations that arise from the singlet $A \leftarrow X$ transition is reduced and the magnitude of the 1 000-nm satellite decreases considerably as the temperature increases. Since this satellite is mainly arising from *bound-bound* transitions, the population of the lower levels diminishes at higher temperatures, leading to the decrease of the peak amplitude. Its intensity at 14 000 K is about a factor of 10^3 less than at 4000 K. On the other hand, as Fig. 7(b) shows, the 510-nm satellite resulting from the triplet $c \leftarrow a$ transition grows very slowly and is remarkably redshifted by approximately 2% in the temperature range 4000–14 000 K. Additionally, it also shows the increase in the magnitude of the blue satellite while the red satellite amplitude decreases.

To the best of our knowledge, there are unfortunately no previous experimental or theoretical studies dealing with the LiH photoabsorption spectra with which one can contrast the computed data. Nevertheless, Allard [58] carried out, upon our request, semiclassical calculations with the LiH potentials of Coxon and Dickinson [34] that we have slightly modified in the short- and long-range internuclear separations. In the wavelength range 750–1200 nm and at three distinct temperatures 4000, 5000, and 6000 K, she could identify with her computational method a satellite near the wavelength 980 nm. For a better comparison of our results with those of Allard [58], we have chosen to plot in Fig. 8 the reduced absorption coefficient at $T = 6\,000$ K. On the whole, the agreement is excellent. In addition, we have reproduced the photoabsorption spectra, around the determined satellite positions, by making use of the RKR potentials of Coxon and Dickinson [34] for the singlet $A \leftarrow X$ transition, and of the *ab initio* data of Boutalib and Gadéa [39] for the

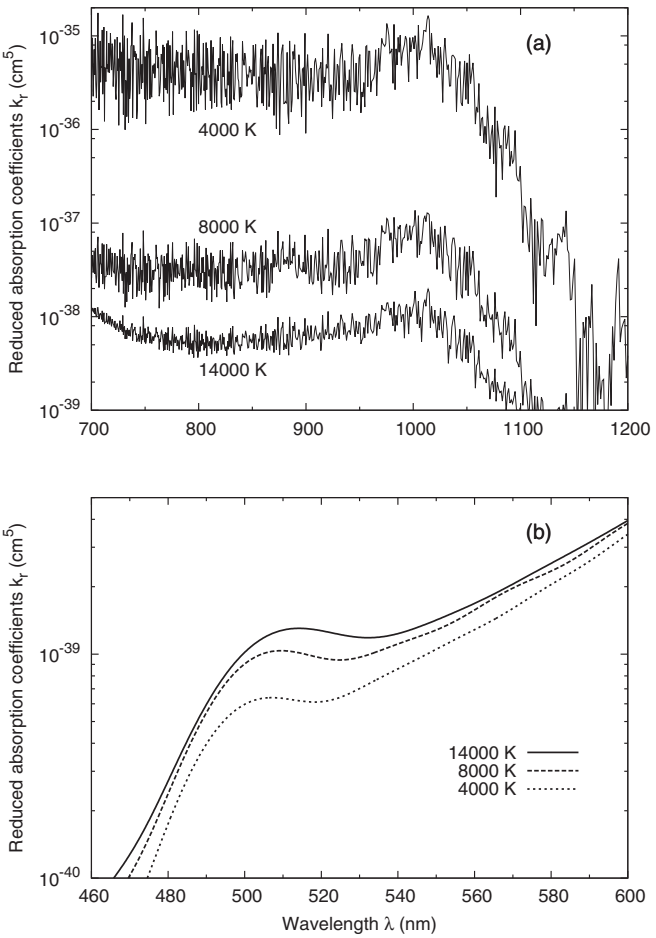

FIG. 7. Temperature effect on the position and intensity of the satellites. Part (a) represents the red-wing satellite and part (b) the blue-wing satellite.

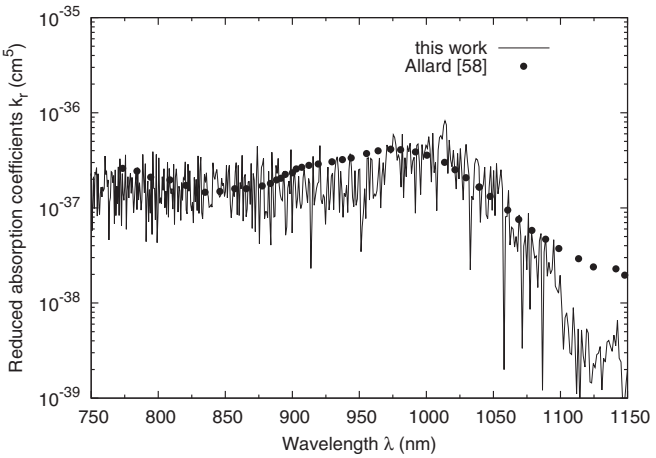

FIG. 8. Comparison between present satellite profile located around $\lambda \sim 1\,000$ nm at $T = 6\,000$ K with that computed by Allard [58].

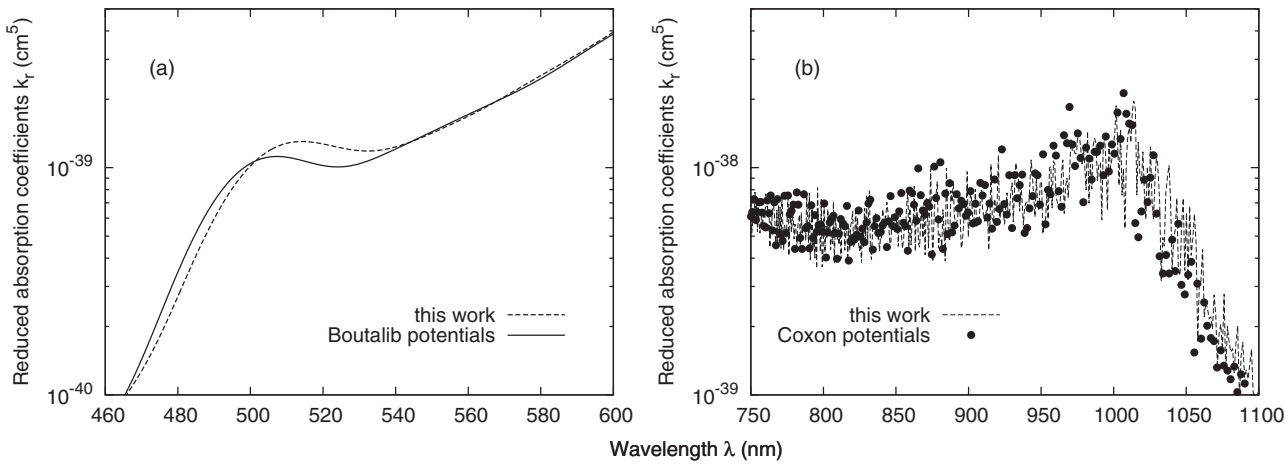

FIG. 9. Blue- and red-wing satellites at $T = 14\,000$ K generated from present potentials and from Boutalib and Gadéa [39] and Coxon and Dickinson [33,34] potentials.

triplet $c \leftarrow a$ transition. As Figs. 9(a) and 9(b) display, the blue- and red-wing satellites generated with the two potential sets are entirely confounded, which essentially demonstrates the accuracy and reliability of the present constructed LiH potentials and TDMs.

VI. CONCLUSION

In this work, the absorption spectra of the radiating Li($2s - 2p$) atoms perturbed by hydrogen H($1s$) has been treated theoretically. The computations have been performed by using the interaction potentials and TDMs, both constructed upon *ab initio* data which we have produced. Their reliability is evaluated by determining the excited-level lifetimes and the rate coefficients for radiative association. Good agreement is obtained in comparison with other published values. The results have specifically shown the sensitivity of the far wings on temperature and the presence of satellite in the red wing, at all temperatures, near the wavelength 1000 nm due to the $A \leftarrow X$ transition. A semiclassical calculation performed by Allard in the wavelength range 750–1200 nm detected the same satellite in the vicinity of 980 nm. The present calculations could also point out the occurrence beyond $T \approx 14\,000$ K of a satellite structure in the blue wing located around 510 nm wavelength generated by the $c \leftarrow a$ transitions.

ACKNOWLEDGMENTS

The authors are very grateful to N. F. Allard, J. A. Coxon, and G.-H. Jeung for all the data points they provided. A part of this work is performed under the PNR project led by the Algerian Ministry of Higher Education and Scientific Research. The Algerian team (N.L., K.A., and M.B.) acknowledges the Ministry's financial support.

[1] A. M. Karo and A. R. Olson, J. Chem. Phys. **30**, 1232 (1959).
[2] P. H. Krupenie, E. A. Mason, and J. T. Vanderslice, J. Chem. Phys. **39**, 2399 (1963).
[3] R. C. Sahni, B. C. Sawhney, and M. J. Hanley, Trans. Faraday Soc. **65**, 3121 (1969).
[4] K. K. Docken and J. Hinze, J. Chem. Phys. **57**, 4928 (1972).
[5] I. L. Cooper and A. S. Dickinson, J. Chem. Phys. **131**, 204303 (2009).
[6] A. Bande, H. Nakashima, and H. Nakatsuji, Chem. Phys. Lett. **496**, 347 (2010).
[7] W.-C. Tung, M. Pavanello, and L. Adamowicz, J. Chem. Phys. **134**, 064117 (2011).
[8] S. Bovino, M. Tacconi, F. A. Gianturco, D. Galli, and F. Palla, Astrophys. J. **731**, 107 (2011).
[9] D. N. Friedel, A. Kemball, and B. D. Felds, Astrophys. J. **738**, 37 (2011).
[10] P. C. Stancil, S. Lepp, and A. Dalgarno, Astrophys. J. **458**, 401 (1996).
[11] E. Bougleux and D. Galli, Mon. Not. R. Astron. Soc. **288**, 638 (1997).
[12] P. C. Stancil and A. Dalgarno, Astrophys. J. **479**, 543 (1997).
[13] F. Combes and T. Wiklind, Astron. Astrophys. **334**, L81 (1998).
[14] A. S. Dickinson and F. X. Gadéa, Mon. Not. R. Astron. Soc. **318**, 1227 (2000).
[15] E. Bodo, F. A. Gianturco, and R. Martinazzo, Phys. Rep. **384**, 85 (2003).
[16] N. F. Allard and J. F. Kielkopf, Rev. Mod. Phys. **54**, 1103 (1982).
[17] J. Szudy and W. E. Baylis, Phys. Rep. **266**, 127 (1996).
[18] H. K. Chung, K. Kirby, and J. F. Babb, Phys. Rev. A **63**, 032516 (2001).
[19] P. Durand and J. C. Barthelat, Theor. Chim. Acta **38**, 283 (1975).
[20] W. Müller and W. Meyer, J. Chem. Phys. **80**, 3311 (1984).
[21] M. Foucrault, P. Millie, and J. P. Daudey, J. Chem. Phys. **96**, 1257 (1992).
[22] M. Korek, A.-R. Allouche, M. Kobeissi, A. Chaalan, M. Dagher, K. Fakherddin, and M. Aubert-Frécon, Chem. Phys. **256**, 1 (2000).
[23] B. Huron, J. P. Malrieu, and P. Rancurel, J. Chem. Phys. **58**, 5745 (1973).

[24] S. Evangelisti, J. P. Daudey, and J. P. Malrieu, Chem. Phys. **75**, 91 (1983).
[25] H. Pauly, in *Atomic-Molecule Collision Theory*, edited by R. B. Bernstein (Plenum, New York, 1979).
[26] J. Mitroy and M. W. J. Bromley, Phys. Rev. A **68**, 062710 (2003).
[27] J. Y. Zhang and J. Mitroy, Phys. Rev. A **76**, 022705 (2007).
[28] J. M. Zhu, B. I. Zhoo, and Z. C. Yan, J. Phys. B **34**, 1535 (2001).
[29] R. J. Le Roy, in *Molecular Spectroscopy* 1 (Chem. Soc. Spec. Periodical), edited by R. F. Barrow, D. A. Long, and D. J. Millin (Chemical Society, London, 1973).
[30] W. C. Stwalley, W. T. Zemke, K. R. Way, K. C. Li, and T. R. Proctor, J. Chem. Phys. **66**, 5412 (1977).
[31] N. Geum, G.-H. Jeung, A. Derevianko, R. Côté, and A. Dalgarno, J. Chem. Phys. **115**, 5984 (2001).
[32] G.-H. Jeung (private communications).
[33] J. A. Coxon and C. S. Dickinson, J. Chem. Phys. **121**, 9378 (2004).
[34] J. A. Coxon (private communication).
[35] W. C. Stwalley and W. T. Zemke, J. Phys. Chem. Ref. Data **22**, 87 (1993).
[36] F. X. Gadéa and T. Leininger, Theor. Chem. Acc. **116**, 566 (2006).
[37] R. Côté, M. J. Jamieson, Z.-C. Yan, N. Geum, G.-H. Jeung, and A. Dalgarno, Phys. Rev. Lett. **84**, 2806 (2000).
[38] J. N. Murrell, T. G. Wright, and S. D. Bosanac, J. Mol. Struct.: Theochem **591**, 1 (2002).
[39] A. Boutalib and F. X. Gadéa, J. Chem. Phys. **97**, 1144 (1992).
[40] Y. C. Chan, D. R. Harding, W. C. Stwalley, and C. R. Vidal, J. Chem. Phys. **85**, 2436 (1986).
[41] K. R. Way and W. C. Stwalley, J. Chem. Phys. **59**, 5298 (1973).
[42] W. L. Wiese, M. W. Smith, and B. M. Glennon, *Atomic Transitions Probabilities*, Vol. 1. Hydrogen through Neon (National Bureau of Standards, Washington, DC, 1966).
[43] W. T. Zemke and W. C. Stwalley, J. Chem. Phys. **68**, 4619 (1978).
[44] H. Partridge and S. R. Langhoff, J. Chem. Phys. **74**, 2361 (1981).
[45] P. J. Dagdigian, J. Chem. Phys. **64**, 2609 (1976).
[46] P. H. Wine and L. A. Melton, J. Chem. Phys. **64**, 2692 (1976).
[47] F. von Moers, S. Heitz, H. Büsener, H.-J. Sagner, and A. Hese, Chem. Phys. **116**, 215 (1987).
[48] J. Carlsson and L. Sturesson, Z. Phys. D **14**, 281 (1989).
[49] W. I. McAlexander, E. R. I. Abraham, and R. G. Hulet, Phys. Rev. A **54**, R5 (1996).
[50] U. Volz and H. Schmoranzer, Phys. Scr., T **65**, 48 (1996).
[51] R. J. Le Roy, N. S. Dattani, J. A. Coxon, A. J. Ross, P. Crozet, and C. Linton, J. Chem. Phys. **131**, 204309 (2009).
[52] A. Kramida, Yu. Ralchenko, J. Reader, and NIST ASD Team, NIST Atomic Spectra Database (ver. 5.0). Available: http://physics.nist.gov/asd National Institute of Standards and Technology, Gaithersburg, MD (2012).
[53] F. A. Gianturco and P. Gori Giorgi, Phys. Rev. A **54**, 4073 (1996).
[54] F. A. Gianturco and P. Gori Giorgi, Astrophys. J. **479**, 560 (1997).
[55] A. Dalgarno, K. Kirby, and P. C. Stancil, Astrophys. J. **458**, 397 (1996).
[56] M. C. Bacchus-Montabonel and D. Talbi, J. Mol. Struct.: Theochem **463**, 91 (1999).
[57] O. J. Bennett, A. S. Dickinson, T. Leininger, and F. X. Gadéa, Mon. Not. R. Astron. Soc. **341**, 361 (2003); **384**, 1743 (2008).
[58] N. F. Allard (private communications).